



**HAL**  
open science

# Homojunction Doping for Efficient Hole Extraction in Polymer Solar Cells

Francis Feaugas, Tommaso Nicolini, Gilles Roche, Lionel Hirsch, Olivier Dautel, Guillaume Wantz

► **To cite this version:**

Francis Feaugas, Tommaso Nicolini, Gilles Roche, Lionel Hirsch, Olivier Dautel, et al.. Homojunction Doping for Efficient Hole Extraction in Polymer Solar Cells. *Solar RRL*, 2023, 7 (2), 10.1002/solr.202200815 . hal-04235875

**HAL Id: hal-04235875**

**<https://hal.science/hal-04235875>**

Submitted on 10 Oct 2023

**HAL** is a multi-disciplinary open access archive for the deposit and dissemination of scientific research documents, whether they are published or not. The documents may come from teaching and research institutions in France or abroad, or from public or private research centers.

L'archive ouverte pluridisciplinaire **HAL**, est destinée au dépôt et à la diffusion de documents scientifiques de niveau recherche, publiés ou non, émanant des établissements d'enseignement et de recherche français ou étrangers, des laboratoires publics ou privés.



Distributed under a Creative Commons Attribution - NonCommercial 4.0 International License

# Homojunction Doping for Efficient Hole Extraction in Polymer Solar Cells

Francis Feugas<sup>a</sup>, Tommaso Nicolini<sup>b</sup>, Gilles H. Roche<sup>a</sup>, Lionel Hirsch<sup>a</sup>, Olivier Dautel<sup>c</sup>, Guillaume Wantz<sup>a</sup>

<sup>a</sup> Univ. Bordeaux, CNRS, Bordeaux INP, IMS, UMR 5218, F-33400, Talence, France

<sup>b</sup> Univ. Bordeaux, CNRS, Bordeaux INP, ISM, UMR 5255, F-33400, Talence, France

<sup>c</sup> Institut Charles Gerhart de Montpellier, CNRS, Université de Montpellier, ENSCM, F-34293, Montpellier, France

## Abstract

**Hole transporting layers** (HTL) in polymer solar cells remains a subject of importance to enable enhanced efficiency and stability compared to the benchmark PEDOT:PSS. We report here the design of an interlayer based on the same polymer as the one used in the bulk heterojunction. In this HTL the polymer is doped, thus forming a so called homojunction. The conductivity of PTQ10 doped with Magic Blue was optimized varying dopant concentration. Resulting solar cells showed competing power conversion efficiency as the widely used PEDOT:PSS and an improved stability. This strategy opens the route towards the development of deep lying work function HTL and is promising for future bulk heterojunction materials with deep lying HOMO polymers.

**Keywords:** Polymer Doping – Organic Photovoltaic – Work Function Tuning – Magic Blue – Homojunction

---

In recent years, progress in improving the performance of **organic photovoltaic (OPV)** cells has been considerable, especially thanks to the development of novel organic semiconductors (OSC)<sup>[1],[2],[3]</sup>. At the same time, the interest in doping OSCs has never stopped growing with versatile applications from energy storage<sup>[4]</sup>, thermoelectrics<sup>[5]</sup> and more generally for organic electronics<sup>[6],[7],[8]</sup>. For OPV solar cells, doping is also attracting attention. Several recent records of power conversion efficiency (PCE) have been achieved by introducing either n-type dopants<sup>[9],[10]</sup> or p-type dopants<sup>[11],[12],[13],[14]</sup> directly into the device bulk heterojunction (BHJ) layer, leading to a maximum PCE of 18.3%<sup>[9]</sup>. Moreover, as the improvement of performance and stability in OPVs has also been possible thanks to interfacial engineering, OSC doping of interlayers can be used as a strategy.

While the selection of materials used as **electron transporting Layers (ETL)** is quite wide<sup>[15]</sup>, this is not the case for **hole transporting layer (HTL)** materials, where the conducting polymer poly(3,4-ethylenedioxythiophene) polystyrene sulfonate (PEDOT:PSS) has established itself as the most popular material due to its relatively high transparency, high conductivity and relatively high work function<sup>[16]</sup>. However, PEDOT:PSS has been shown to be responsible for several stability issues in devices, especially due to its strong acidity that can cause material degradation<sup>[17]</sup>, including ITO etching<sup>[18]</sup>. PEDOT:PSS is also known to form a mechanically poor interface with the bulk heterojunction active layer inducing premature delamination of flexible solar cells, when subjected to mechanical strains, especially for industrial fabrication processes such as roll-to-roll technique<sup>[19]</sup>. These drawbacks push for the need to develop novel hole extraction strategies and materials for OPV solar cells.

In the growing field of hybrid perovskite p-i-n solar cells (PSC), p-doped semiconducting polymers like tris(pentafluorophenyl)borane-doped poly[bis(4-phenyl)(2,4,6-trimethylphenyl)amine (PTAA)<sup>[20]</sup> can be easily used as an efficient HTL due to the solvent orthogonality when depositing the hybrid perovskite layer onto PTAA. Such interlayer cannot be used for **conventional OPV cells (p-i-n)** because most of the organic solvents used to deposit the bulk heterojunction are also good solvents for the doped-PTAA, with the risk of dissolving and degrading the bottom layer. To overcome this issue, Shu *et al.*<sup>[21]</sup> developed in 2013 a method to stack two layers of polymer by depositing them on two different substrates prior to lamination. This technique enabled to produce **conventional OPV structures** using poly(3-hexylthiophene) (P3HT) doped with Mo(tfd-CO<sub>2</sub>Me)<sub>3</sub> in homojunction with a P3HT:PC<sub>61</sub>BM active layer, showing similar performances to those made with the PEDOT:PSS HTL<sup>[22]</sup>. The term “homojunction” here stands on the fact of using the same polymer in the HTL and the active layer, as the same p-type polymer is used in both. Another alternative to classic heterojunction HTLs in OPV is to employ sequential doping of the active layer in inverted devices (n-i-p). By doping the top of the active layer, efficient hole collection is achieved at the anode without the use of a dedicated additional HTL. In 2014, Guillain *et al.* successfully solution-deposited a F4TCNQ layer onto a P3HT:PCBM active layer<sup>[23]</sup>, sparking interest for this promising approach. However, this process cannot be easily implemented at the industrial scale for large area printing. Moreover, F4TCNQ is not necessarily an efficient dopant for some recent semiconducting polymers with deep-lying HOMO levels. Furthermore, controlling the depth of penetration of the dopant molecules into the active layer seems to be a major issue in the fabrication of such devices<sup>[24]</sup>. Several other recent attempts to replace PEDOT:PSS have shown promising results. In 2019, Lin *et al.* successfully improved the PCE of devices with several active layers by using a liquid exfoliated transition metal dichalcogenide WS<sub>2</sub><sup>[25]</sup>. At the same time, an interest appeared in the use of Self-Assembled Monolayers (SAM) in OPVs, that allowed to achieve high PCE of 18.4%. However, the stability of such devices have not yet been fully investigated<sup>[26]</sup>. Finally, Xu *et al.* have reported devices exhibiting better performances and stability using a new, less acidic and solution processable polymer called PCPDT-2Ph-H<sup>[27]</sup>.

Here we demonstrate the fabrication of solution-processed **conventional (p-i-n) OPV structure** embedding an HTL consisting of the same polymer used in the active layer: Poly[[6,7-difluoro[[2-hexyldecyl)oxy]-5,8-quinoxalinediyl]-2,5-thiophenediyl] (PTQ10, **Figure 1a**), a recent major polymer candidate for OPV with simplified chemical structure and lower cost synthesis<sup>[28]</sup>. Against the rules of solvent orthogonality, we show that coating the polymer:NFA (Non-Fullerene-Acceptor) bulk heterojunction on top of the HTL consisting of doped PTQ10 is feasible. The well-known p-type dopants such as F4TCNQ cannot efficiently dope the deep lying HOMO donor polymer PTQ10 (-5.54 eV<sup>[28]</sup>) because they do not display a deep enough LUMO level (-5.24 eV<sup>[29]</sup>). Thus, the chosen dopant is the strong oxidant tris(4-bromophenyl)ammoniumyl hexachloroantimonate, shown in **Figure 1a**, also known as *Magic Blue* (MB) for its intense dark blue color. It has been recently used to dope polymers with deep lying HOMO level down to -5.8 eV<sup>[30]</sup>. MB-doped PTQ10 shows improved electrical conductivity and work function (WF) allowing an efficient extraction of charges. This layer is used in **conventional OPV architectures** with a PTQ10:ITIC-4F active layer. ITIC-4F (3,9-bis(2-methylene-((3-(1,1-dicyanomethylene)-6,7-difluoro)-indanone))-5,5,11,11-tetrakis(4-hexylphenyl)-dithieno[2,3-d:2',3'-d']-s-indaceno[1,2-b:5,6-b']dithiophene, **Figure 1a**) is a recognized Non Fullerene Acceptor (NFA) exhibiting good performances when mixed with a fluorinated donor polymer<sup>[31],[32]</sup> including PTQ10<sup>[33]</sup>. The resulting solar cells performances are competing with those obtained with the reference material PEDOT:PSS. **Time-of-flight secondary ion mass spectrometry** (ToF-SIMS) measurements showed that the vertical composition of the device is preserved despite forming the homojunction between the active layer and the HTL. No unwanted diffusion of species between layers is observed, suggesting that such solar cells present promising stability.

## **Materials & Methods**

PTQ10 and ITIC-4F were purchased from *Brilliant Matters*. PDINO was purchased from *1-Material*. PEDOT:PSS *Clevios PH* was purchased from *Heraeus*. MB was purchased from *Sigma Aldrich*. Thicknesses of all layers > 30 nm were measured with the *Alpha-Step IQ* surface profilometer from *KLA-Tencor*. Thickness of ultra-thin HTL films was estimated by UV-vis absorbance spectroscopy comparing their absorbance with the absorbance of a thicker film made of the same material. ITO coated glass (10  $\Omega$ /sq) were successively ultrasonically cleaned with a basic solution, deionized water, and isopropanol. An additional 15min UV-Ozone treatment was applied only to the reference PEDOT:PSS devices. For MB-doped PTQ10 deposition, ITO substrates did not require any UV-ozone treatment to be well-covered by the solution. PEDOT:PSS was spin-coated at 3000 rpm – 1000 rpm/s during 45 s and subsequently annealed at 130 °C during 30 min to provide  $43 \pm 3$  nm thick layers. Magic Blue solutions with various concentrations in acetonitrile (ACN) were introduced in PTQ10 solutions in cyclopentyl methyl ether (CPME) with a ACN:CPME ratio of (1:7.5). The doped solutions were spin-coated at 3000 rpm during 60s and dried 5 min at 110 °C to obtain  $7 \pm 1$  nm thick layers. Active layer composed of PTQ10:ITIC-4F (1:1) at 16 mg/mL in chloroform was spin-coated at 1400 rpm during 60 sec then annealed 5min at 80 °C. PDINO at 1 mg/mL in methanol was spin-coated at 3500 rpm during 60 s. 100 nm-thick Al electrodes were thermally evaporated under secondary vacuum ( $10^{-6}$  mbar). An active area of 10.5 mm<sup>2</sup> was defined through the use of a shadow mask for the evaporation. All devices performance measurements were characterized at room temperature under nitrogen atmosphere using *Keithley 2400* under AM 1.5G illuminations (1000 W/m<sup>2</sup>) provided by a *LCS-100* solar simulator from *Oriel* and calibrated using a Silicon KG5 cell. The performances were measured for 8 different devices for all samples, and 16 samples for the devices made with PTQ10 doped with 20%mol of MB (estimated vs PTQ10 monomer). UV-Vis NIR absorbance spectra were obtained using a *Shimadzu UV-3600 Plus* spectrophotometer. AFM images were obtained in tapping mode using a *Innova* Microscope from *Bruker*. UV-Vis-NIR spectroelectrochemical conductance measurements were performed according to a method recently proposed<sup>[34]</sup>. Two *PalmSense4* potentiostats were used to perform electrochemical cycling and conductance measurements while a *Black Comet CSR-XR* compact spectrophotometer equipped with optical fibers and collimating lenses were used to record the evolution of PTQ10 conductivity upon electrochemical doping. Conductivity of Magic Blue-doped PTQ10 was measured between 2 gold electrodes of 5 mm with a gap of 0.5 mm. Electrodes were thermally evaporated on top of the film and 6 different IV measurements were realized and averaged. Kelvin Probe measurements were performed using a Kelvin Control 07 from *Besocke Delta Phi* and a gold cantilever and Highly Oriented Pyrolytic Graphite (HOPG) as a calibration sample (with an assumed work function of 4.6 eV)<sup>[35]</sup>. ToF-SIMS measurements were performed using a ToF-SIMS 5 from *IonTof*, with negative ion depth profiles, using a 500 eV O<sub>2</sub> source on a 300 x 300  $\mu$ m<sup>2</sup> surface for sputtering and a 30 kV Bi+ source on a 100 x 100  $\mu$ m surface for analysis.

## **Results and discussion:**

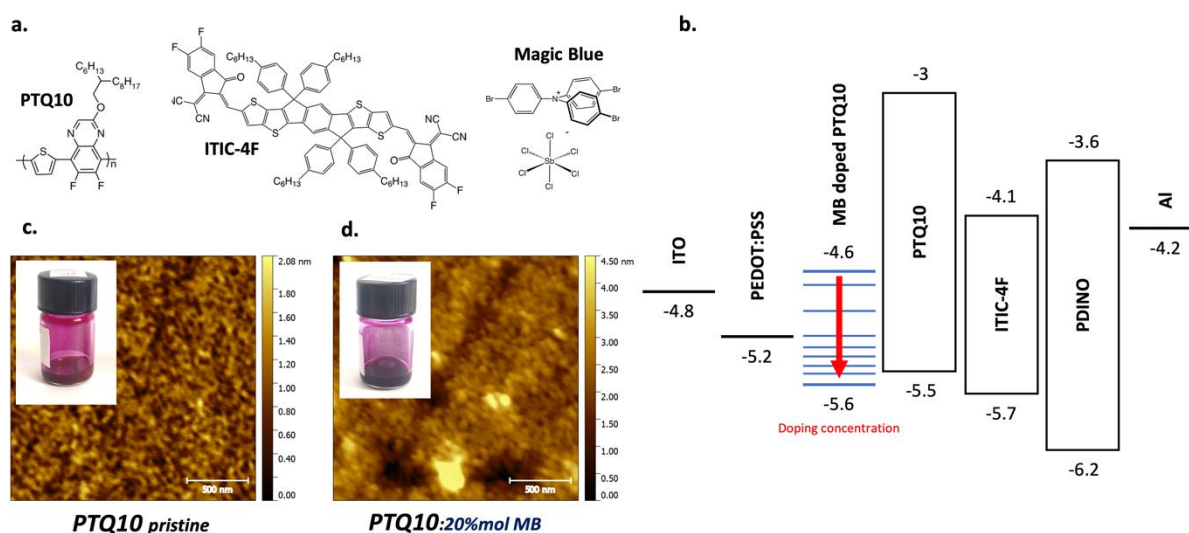


**Figure 1:** a) Molecular structures of materials; b) Energy levels of materials, note that doped PTQ10 values are experimental from Kelvin probe measurements performed in the present study; AFM images of c) Pristine PTQ10 and d) PTQ10 doped with 20%mol of Magic Blue (inset show photographs of undoped and doped PTQ10 solutions).

**Figure 1** shows photographs of the undoped PTQ10 solution and PTQ10 with 20%mol of MB. As can be seen, upon the introduction of Magic Blue into the PTQ10 solution, the solution turns from light purple to dark purple. UV-Vis-NIR absorption spectra of corresponding thin films are shown in **Figure 2a**. Upon addition of MB, two distinct polaronic signatures are observed. The PTQ10 absorption feature at 500-580 nm progressively disappears as dopant concentration is increased. The polaronic absorption peaks are described as a wide peak between 700 and 920 nm and a well-delocalized broad feature in the infrared region. Those optical changes upon the introduction of Magic Blue are typical of Pi-conjugated polymer doping and similar to those observed for the sequential doping of others polymers<sup>[30]</sup>. At large dopant concentration, the spectra attest to the oxidation of a large fraction of the oxidizable sites of PTQ10. The UV-Vis-NIR spectra of an ACN solution of pure MB is also shown in **Figure 2a** (blue curve). Its absorption band localized at 780 nm in the same area of the polaronic peak of the doped PTQ10 thin film could lead to consider the band observed in the film as the result of the presence of a high amount of MB instead of a polaronic peak of the doped PTQ10. To determine whether the peak between 700 and 920 nm is due to the presence of MB, or characteristic of polaron formation, we performed spectroelectrochemical UV-Vis-NIR spectroscopy of the doped PTQ10 films. Using a transparent solution of tetrabutylammonium perchlorate (TBAP), we applied a potential on the film versus a silver pseudo reference and measured the transmittance variation while performing cyclic voltammetry. In **Figure 2c**, the optical density variation,  $\Delta OD$ , across the UV-Vis-NIR spectrum, for the polymer in neutral, partially oxidized, and highly oxidized is reported. Those measurements clearly show decrease of transmittance between 500 nm and 650 nm and the concurrent appearance of a new band between 650 nm and 950 nm, corresponding respectively to the collapsing of the neutral absorption band of the polymer and the creation of the polaronic band visible on the **Figure 2a**. **Figure 2b** examines the dopant concentration threshold for which a significant contribution is observable on the spectroscopic signature of polarons. As it can be seen following the evolution of the normalized absorbance of the neutral state peak (580 nm) and the polaronic peaks (850 nm and 1465nm), the doping effect becomes significantly visible in UV-Vis spectroscopy for doping ratios higher than 10%mol.

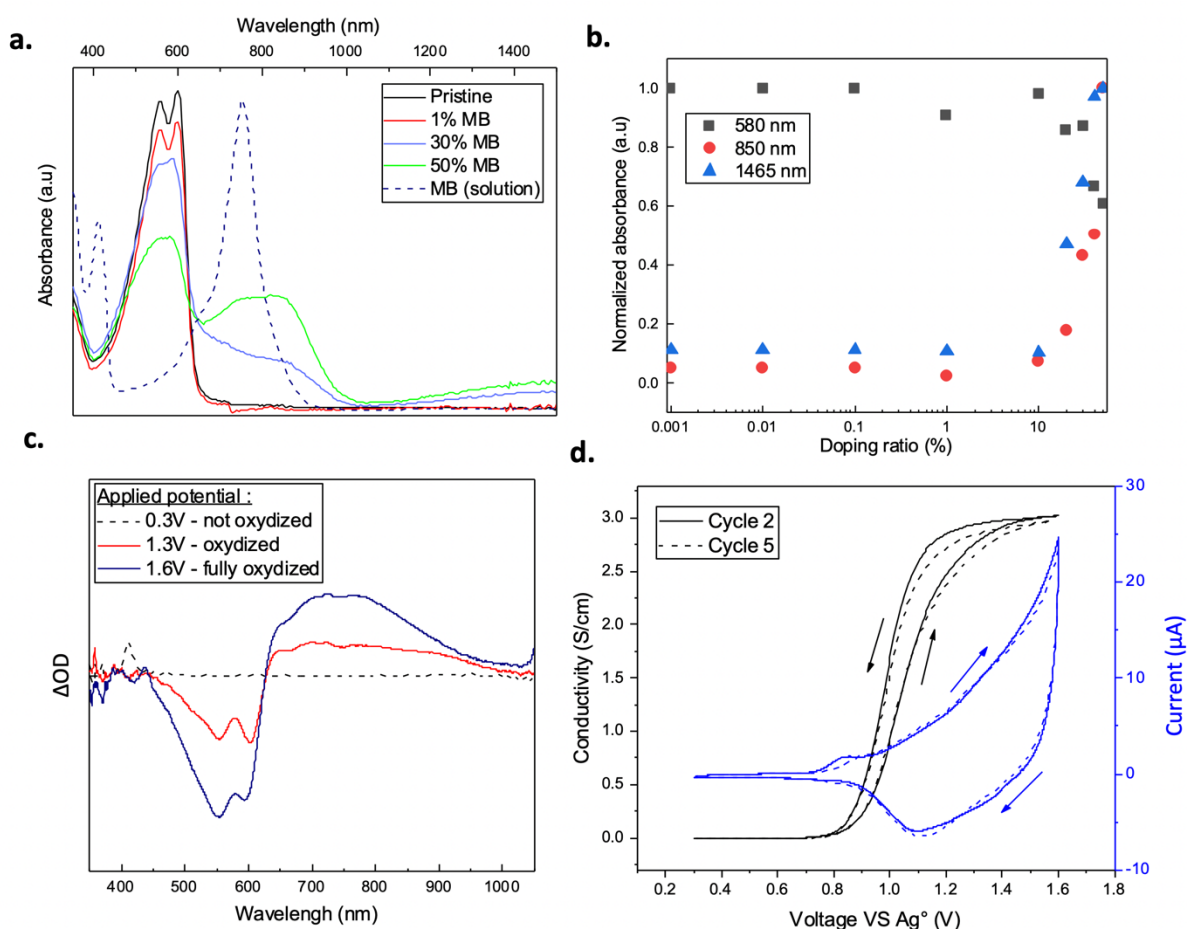


**Figure 2: a) Absorption spectra of pristine and doped PTQ10 films for various MB concentrations. b) Evolution of the normalized absorbance at 580, 850 and 1465nm as a function of doping concentration c) UV-Vis electrochemical spectroscopy spectra d) C-V cyclic curve and evolution of conductivity during electrochemical cycling of PTQ10.**

The impact of doping on the morphology of the PTQ10 films was studied by Atomic Force Microscopy (AFM). The **Figure 1c** and **Figure 1d** shows the height profile of pristine and 20%mol doped PTQ10. There is a clear formation of aggregates upon the introduction of dopant in high amount. This phenomenon, inherent to bulk doping, was a limit to the processing of PTQ10 solutions with a doping ratio over 50%mol and has previously been reported as a possible limit of bulk doping at high concentrations<sup>[36],[37]</sup>.

The **Figure 3a** shows the electrical conductivity of doped PTQ10 films from 10%mol to 50%mol. Due to our measurement device sensibility limited to approximately  $10^{-6}$  S/cm, attempts to measure the conductivity of pristine PTQ10 and doped PTQ10 at low concentration from 0.01%mol to 1%mol was not successful. This result confirms that the polymer, as received, is well purified and not significantly doped by any impurity from the chemical synthesis<sup>[38]</sup>. **The maximum conductivity of 0.13 S/cm is achieved for 30%mol MB concentration which represents an increase of the conductivity of at least five orders of magnitude compared to pristine PTQ10.** In order to estimate the efficiency of chemical doping obtained with Magic Blue from solution processing, we performed electrochemical conductance measurements on pristine PTQ10 films on interdigitated electrode as the working

electrode of an electrochemical cell. This doping process occurs through the oxidation of PTQ10, which is accompanied by anion injection and concurrent swelling of the polymer structure. We therefore expect to obtain the maximum achievable doping of PTQ10 and conductivity in the explored potential window, limited only by the electrochemical stability of the electrolytic solution and of the polymer. The evolution of the conductivity during electrochemical doping is shown on **Figure 2d**. The achieved maximum conductivity of electrochemically doped PTQ10 saturates at around 3 S/cm above applied potential difference of 1.5 V, suggesting that all sites contributing to electrical charge transport are efficiently doped. This value is relatively higher than the 0.13 S/cm obtained with 20%mol doping ratio. Indeed, the 3 S/cm value may represent a maximum conductivity value of electrochemically doped PTQ10 which is not easily achievable through bulk doping by molecular dopants through solution processing. In fact, for doped PTQ10 films with doping ratios higher than 20%mol, the conductivity saturates and eventually decreases. This phenomenon, not in line with the polaronic spectroscopic data, could be due to the growth of aggregates at high dopant concentration, as observed on AFM images, hindering charge transport through the doped polymer film. Similar behavior has already been reported for solution doping cases with different polymers and dopants, like PTBTTT-c doping by  $\text{Mo}(\text{tfd-COCF}_3)_3$ <sup>[37]</sup> or P3HT doping by F4TCNQ<sup>[39]</sup>. It is also important to mention that the new HTL created by doping the PTQ10 does not necessarily need to show record conductivity values when it comes to the development an efficient HTL for OPV solar cells. It is related to the HTL layer thickness which, in general, remains low to enable maximized light transmission. For example, Fu et al. modified the PEDOT:PSS, resulting in modifications of its conductivity, and obtain good performances for PEDOT:PSS with conductivities of  $7.85 \times 10^{-4}$  S/cm<sup>[40]</sup>. Moreover, an anodic current was recorded, corresponding to the oxidation of the polymer, while the increase of the conductivity occurred. It confirms that positive charges are injected into the film and then, that p-type doping occurred without a molecular dopant.

Kelvin Probe was used to measure the work function (WF) at the surface of the doped PTQ10 films deposited on ITO coated glass substrates. The results on **Figure 3b** shows significant increased WF values upon doping. For the 20%mol MB doped PTQ10, it reaches the value of 5.23 eV, matching the reference value of PEDOT:PSS, also measured internally. WF of ITO coated with highly doped PTQ10 surpasses PEDOT:PSS-coated ITO up to 5.58 eV. Such values are very promising for the OPV HTL application since the highest WF difference between the anode and the cathode, is a pre-requisite for maximizing the open-circuit voltage ( $V_{oc}$ ) of solar cells<sup>[41]</sup>.

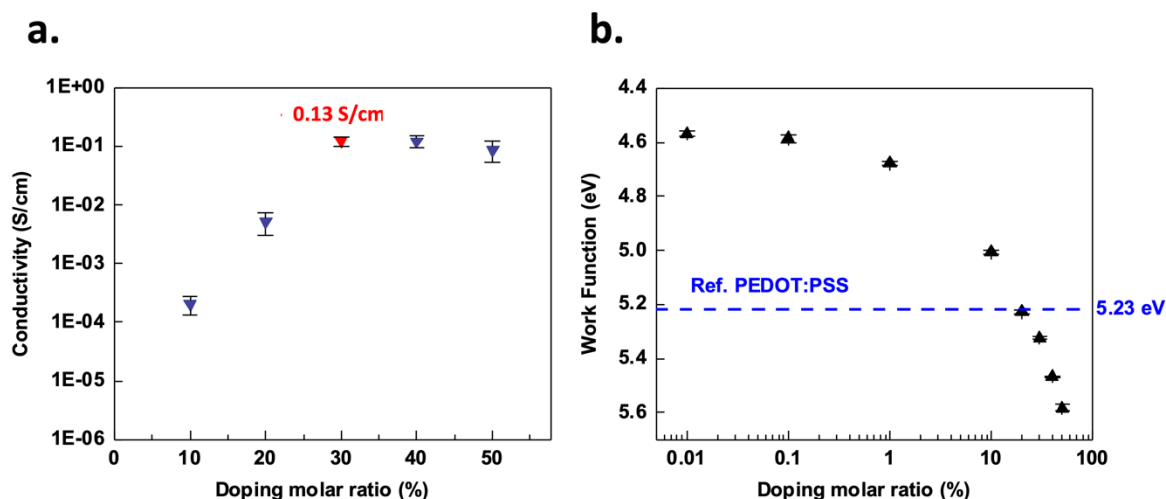


**Figure 3: a) Conductivity of doped PTQ10 films versus doping molar ratio. b) Work function of ITO coated by doped PTQ10 films versus doping molar ratio.**

Although it might seem unusual to deposit an active layer on an interlayer without respecting the solvent orthogonality, functional devices were obtained. Indeed, after having carefully evaporated the CPME used to deposit the doped PTQ10, thanks to a thermal annealing at 110 °C for 5 min, the active layer is deposited from chloroform, a highly volatile solvent, in order to avoid its penetration in the HTL. The expected structure of the resulting device is shown in **Figure 4a**.

To ensure that dopants from the HTL were not washed away from the polymer during the deposition process of the active layer or that the whole HTL deposited remained, ToF-SIMS measurements were performed on the ITO/PTQ10:20%mol Magic Blue/BHJ stack deposited in the same conditions including thermal annealing before and after the deposition of the BHJ layer and are shown in **Figure 4b**. Monitoring the signals for bromine and chlorine ions (present in the cation and anion of Magic Blue, respectively) allows to localize the dopant in the thin film layer structure. As shown on the figure, the dopants are clearly localized into the HTL. No diffusion of dopant into the active layer is observed even when the stack has been annealed. Consequently, the actual vertical composition of the device is close to the expected one, drawn on **Figure 4a**. From this data, we cannot however exclude the possible diffusion of the NFA acceptor into the HTL, which is not traceable with this characterization method considering that PTQ10 and ITIC-4F contain the same elements. However, if a significant amount of NFA were to migrate into the HTL it may hindered the solar cells from working properly, which is not the case here.

The apparent stability of the stacked layer structure could be explained by the quick deposition and evaporation of the BHJ solution coupled with the phenomenon of increased pi-stacking occurring between the polymer chains upon doping. This effect was previously reported on polymers such as P3HT<sup>[42]</sup>, and more recently exploited by Zokaei et al. to increase the elastic modulus of p(g42T-T) and P3DDT upon doping<sup>[43]</sup>. Moreover, dopant diffusion in a polymer matrix is a major cause of doping instability as reported for the Mo(tfd-CO<sub>2</sub>Me)<sub>3</sub> doping of P3HT<sup>[44]</sup>. We performed similar ToF-SIMS measurements realized in the exact device fabrication conditions with thermal annealing after BHJ deposition at 80 °C for 5 min. Results were compared on the same device stack, without thermal annealing and after a higher thermal annealing of 110 °C during 10 min (see **Figure S1** and **Figure S2**). No significant changes neither in the position nor the thickness of the Magic Blue signals were observed. We conclude that the vertical diffusion of the dopant seems to be kinetically impaired

under the explored conditions in such devices. This could be due to a blocking effect of the acceptor at the interface between HTL and active layer as mentioned in a previous study<sup>[44]</sup>.

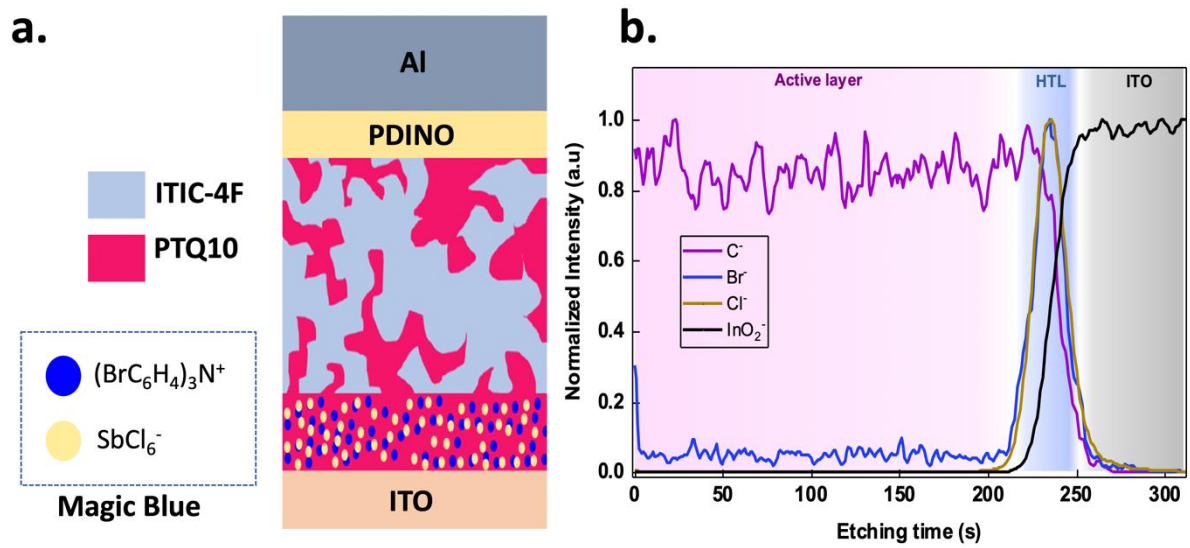


Figure 4: a) Schematic representation of the obtained architecture of the cell. b) ToF-SIMS measurements of the HTL and active layer stack deposited on ITO.

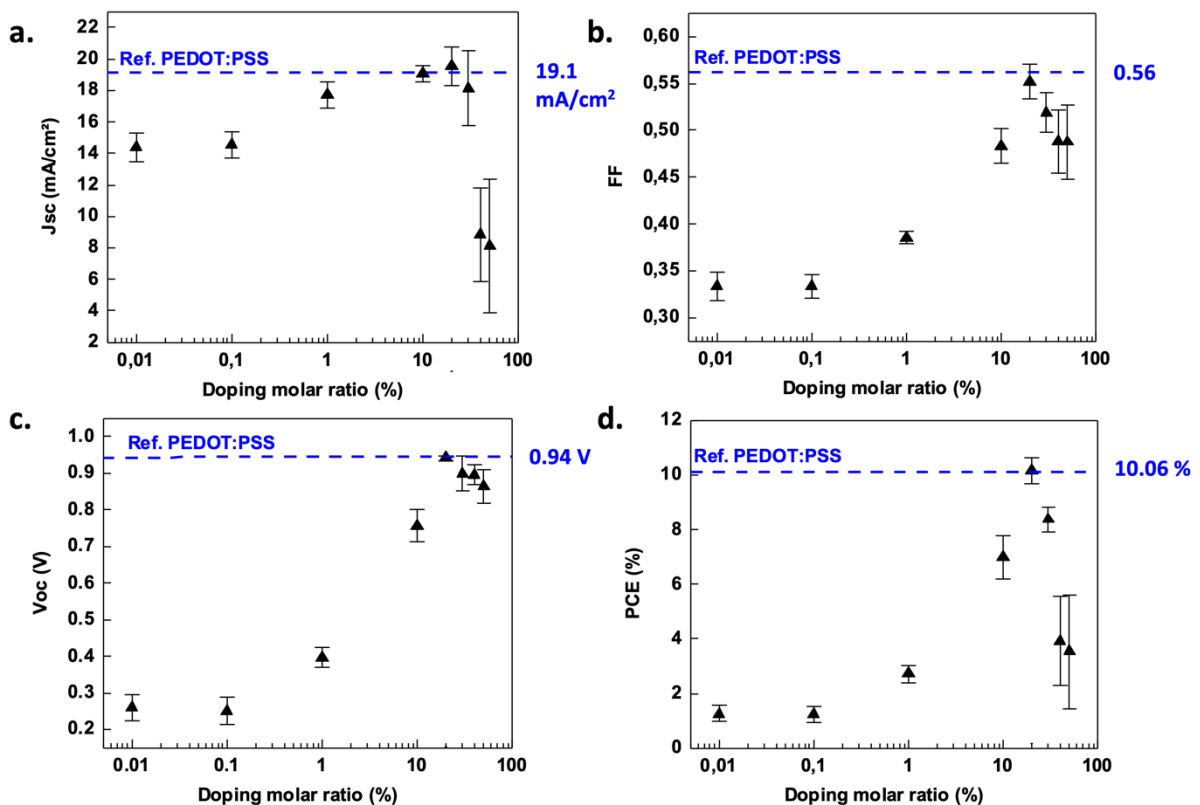


Figure 5: Solar cell parameters as a function of doping concentration in the PTQ10 interlayer. a) Short-circuit current density  $J_{sc}$  b) fill factor FF c) open-circuit voltage  $V_{oc}$  and d) power conversion efficiency PCE – blue mark is a guideline for the eye representing the reference PEDOT:PSS based solar cells.

After having successfully realized PTQ10-doped HTL with increased work function, improved conductivity and having successfully stacked the BHJ on top of the HTL, complete OPV devices were prepared in **conventional (p-i-n) architecture**. Devices with PTQ10 doped from 0.01% to 50%mol were compared with reference devices with PEDOT:PSS. The HTL layer thickness was first carefully optimized to minimize light absorption by PTQ10. Device performances as a function of HTL thickness are shown on **Figure S3**. The short-circuit current density ( $J_{sc}$ ) is strongly affected by the thickness of the HTL. The optimal thickness of the doped PTQ10 layer was found to be between 6 nm and 8 nm and it was kept constant for the following investigations. **Figure 5** shows the resulting PV parameters as a function of the dopant concentration. HTLs with low dopant concentration lead to inefficient devices suffering from low open-circuit voltage ( $V_{oc}$ ) and low fill factor (FF). Inadequate HTL work function, *i.e.*, not deep enough with respect to the HOMO of PTQ10, is penalizing the  $V_{oc}$ . Insufficient HTL conductivity leads to increased series resistances, inducing low FF. Increasing dopant concentration gradually, both the  $V_{oc}$  and the FF increase. For a dopant concentration of 20%mol, the performances are maximized. The  $V_{oc}$  reaches 0.94 V which is comparable to the  $V_{oc}$  for PEDOT:PSS reference sample. Such  $V_{oc}$  is consistent with the state-of-the-art for PTQ10:NFA based solar cells<sup>[33]</sup>. The  $J_{sc}$  of 20 mA/cm<sup>2</sup> shows efficient charge extraction. Combined with a FF of  $0.58 \pm 0.02$ , the optimized PCE is 11.3 %. Such efficiency is competing with the PEDOT:PSS-based reference cells as can be seen on **Figure 6a** comparing the J-V curves of both devices. **Table 1** summarizes the device performances. Magic blue containing devices show good reproducibility despite the non-orthogonality of solvents during the fabrication process. For doping ratio higher than 20%mol, much larger standard deviations are observed especially on the short-circuit currents. The proposed explanation is that the rough morphology of the over-doped layers is detrimental to device performance, either promoting charge recombination in the HTL or presenting of defects at the homojunction interface between the HTL and the active layer. This is consistent with the inhomogeneity of layers observed by AFM (**Figure 1d**). The stability of devices was examined in dark conditions in inert atmosphere and is shown on **Figure 6b**. After 340 h, the doped-PTQ10 based devices retain almost 95% of their initial performances. They are more stable than devices containing PEDOT:PSS whose performance decreases to 82% over the same period. **According to the stability evolution of  $V_{oc}$ ,  $J_{sc}$  and FF shown in Supplementary Informations (Figure S4, S5, S6), this PCE stability improvement is due to a simultaneous slight improvement of the stability of the three PV parameters.**

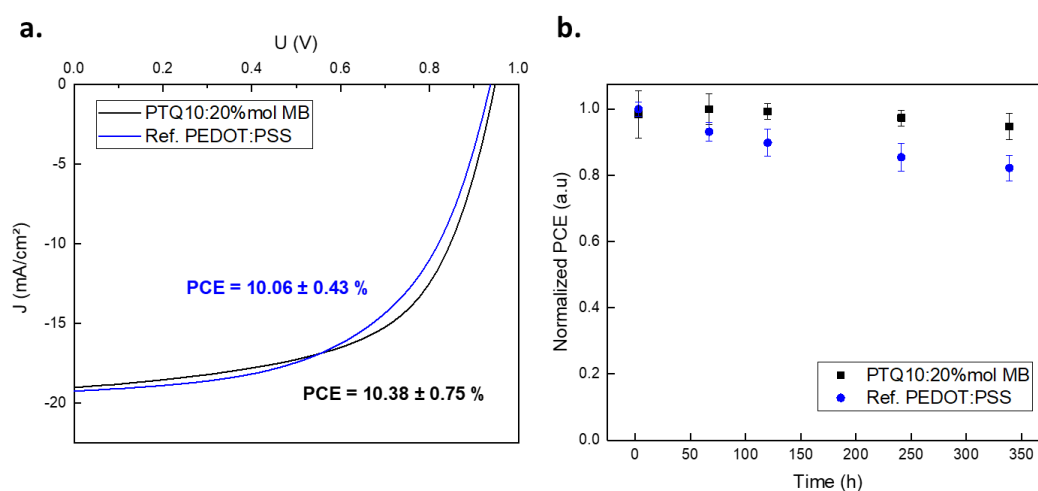


Figure 6: a) J-V curve of best device compared with Ref. PEDOT:PSS device. b) Device stability under inert atmosphere

**Table 1: Photovoltaic parameters (maximum and average values) as function of HTL dopant concentration, compared with PEDOT: PSS reference devices**

| Sample           | $V_{oc}^{max} (V_{oc}^{avg})$ [V] | $J_{sc}^{max} (J_{sc}^{avg})$ [mA/cm <sup>2</sup> ] | $FF^{max} (FF^{avg})$ | $PCE^{max} (PCE^{avg})$ [%] |
|------------------|-----------------------------------|---|-----------------------|-----------------------------|
| PTQ10 : 0.01% MB | 0.31 ( 0.26 ± 0.04 )              | 15.53 ( 14.38 ± 0.90 )                              | 0.36 ( 0.33 ± 0.01 )  | 1.69 ( 1.26 ± 0.29 )        |
| PTQ10 : 0.1% MB  | 0.29 ( 0.25 ± 0.04 )              | 15.24 ( 14.54 ± 0.83 )                              | 0.34 ( 0.33 ± 0.01 )  | 1.52 ( 1.23 ± 0.29 )        |
| PTQ10 : 1% MB    | 0.43 ( 0.40 ± 0.03 )              | 18.53 ( 17.71 ± 0.87 )                              | 0.39 ( 0.39 ± 0.01 )  | 3.04 ( 2.71 ± 0.31 )        |
| PTQ10 : 10% MB   | 0.81 ( 0.76 ± 0.04 )              | 19.83 ( 19.07 ± 0.54 )                              | 0.51 ( 0.48 ± 0.02 )  | 8.06 ( 6.99 ± 0.79 )        |
| PTQ10 : 20% MB   | 0.95 ( 0.94 ± 0.01 )              | 19.81 ( 18.90 ± 0.78 )                              | 0.61 ( 0.58 ± 0.02 )  | 11.25 ( 10.38 ± 0.75 )      |
| PTQ10 : 30% MB   | 0.94 ( 0.90 ± 0.05 )              | 21.00 ( 18.11 ± 2.38 )                              | 0.54 ( 0.52 ± 0.02 )  | 8.92 ( 8.37 ± 0.45 )        |
| PTQ10 : 40% MB   | 0.93 ( 0.90 ± 0.03 )              | 12.78 ( 8.83 ± 3.01 )                               | 0.53 ( 0.49 ± 0.03 )  | 6.27 ( 3.93 ± 1.63 )        |
| PTQ10 : 50% MB   | 0.93 ( 0.86 ± 0.05 )              | 13.74 ( 8.14 ± 4.23 )                               | 0.53 ( 0.49 ± 0.04 )  | 6.54 ( 3.53 ± 2.08 )        |
| Ref. PEDOT:PSS   | 0.94 ( 0.94 ± 0.00 )              | 19.75 ( 19.08 ± 0.48 )                              | 0.58 ( 0.56 ± 0.01 )  | 10.64 ( 10.06 ± 0.43 )      |

## Conclusions

A novel and efficient alternative to PEDOT:PSS in conventional architecture organic solar cells is reported. This is the first time a hole transport layer is designed based on doping the same polymer as the one used in the bulk heterojunction thus forming a so called homojunction. PTQ10 doped by Magic Blue was optimized to tune its conductivity and significantly increase its work function. Resulting solar cells showed competing power conversion efficiency as the widely used PEDOT:PSS and an improved stability. This homojunction strategy opens the route to be applied to future polymers to come in the OPV field. Especially, with the actual tendency to use deep lying HOMO polymers, classical HTL like PEDOT:PSS may not be appropriate to maximize the open-circuit voltage because of its work function. The homojunction doping strategy of using the same polymer in the HTL and in the active layer enables to insure an HTL with a deeper work function than the HOMO level of the polymer. As a consequence, this strategy may become a versatile method for future high efficiency polymer solar cells.

## REFERENCES

- [1] J. Zhang, H. S. Tan, X. Guo, A. Facchetti, H. Yan, *Nat. Energy* **2018**, 3, 720.
- [2] Y. Lin, F. Zhao, Q. He, L. Huo, Y. Wu, T. C. Parker, W. Ma, Y. Sun, C. Wang, D. Zhu, A. J. Heeger, S. R. Marder, X. Zhan, *J. Am. Chem. Soc.* **2016**, 138, 4955.
- [3] Y. Cui, H. Yao, J. Zhang, T. Zhang, Y. Wang, L. Hong, K. Xian, B. Xu, S. Zhang, J. Peng, Z. Wei, F. Gao, J. Hou, *Nat. Commun.* **2019**, 10, 1.
- [4] A. M. Bryan, L. M. Santino, Y. Lu, S. Acharya, J. M. D'Arcy, *Chem. Mater.* **2016**, 28, 5989.
- [5] S. N. Patel, A. M. Glauddell, D. Kiefer, M. L. Chabinyk, *ACS Macro Lett.* **2016**, 5, 268.
- [6] W. Zhu, Y. Mo, M. Yuan, W. Yang, Y. Cao, *Appl. Phys. Lett.* **2002**, 80, 2045.

- [7] G. Lu, J. Blakesley, S. Himmelberger, P. Pingel, J. Frisch, I. Lieberwirth, I. Salzmann, M. Oehzelt, R. Di Pietro, A. Salleo, N. Koch, D. Neher, *Nat. Commun.* **2013**, *4*, 1588.
- [8] A. Ramanavičius, A. Ramanavičiene, A. Malinauskas, *Electrochim. Acta* **2006**, *51*, 6025.
- [9] Y. Lin, M. I. Nugraha, Y. Firdaus, A. D. Scaccabarozzi, F. Aniés, A. H. Emwas, E. Yengel, X. Zheng, J. Liu, W. Wahyudi, E. Yarali, H. Faber, O. M. Bakr, L. Tsetseris, M. Heeney, T. D. Anthopoulos, *ACS Energy Lett.* **2020**, *5*, 3663.
- [10] Y. Lin, Y. Firdaus, M. I. Nugraha, F. Liu, S. Karuthedath, A. H. Emwas, W. Zhang, A. Seitkhan, M. Neophytou, H. Faber, E. Yengel, I. McCulloch, L. Tsetseris, F. Laquai, T. D. Anthopoulos, *Adv. Sci.* **2020**, *7*, 1.
- [11] D. Zhang, Q. Li, J. Zhang, J. Wang, X. Zhang, R. Wang, J. Zhou, Z. Wei, C. Zhang, H. Zhou, Y. Zhang, *ACS Appl. Mater. Interfaces* **2020**, *12*, 667.
- [12] H. Yan, J. Chen, K. Zhou, Y. Tang, X. Meng, X. Xu, W. Ma, *Adv. Energy Mater.* **2018**, *8*, 1.
- [13] Y. Xiong, L. Ye, A. Gadisa, Q. Zhang, J. J. Rech, W. You, H. Ade, *Adv. Funct. Mater.* **2019**, *29*, 1.
- [14] Y. Zhang, H. Zhou, J. Seifert, L. Ying, A. Mikhailovsky, A. J. Heeger, G. C. Bazan, T. Q. Nguyen, *Adv. Mater.* **2013**, *25*, 7038.
- [15] L. Tian, Q. Xue, Z. Hu, F. Huang, *Org. Electron.* **2021**, *93*, 106141.
- [16] K. Sun, S. Zhang, P. Li, Y. Xia, X. Zhang, D. Du, F. H. Isikgor, J. Ouyang, *J. Mater. Sci. Mater. Electron.* **2015**, *26*, 4438.
- [17] J. Cameron, P. J. Skabara, *Mater. Horizons* **2020**, *7*, 1759.
- [18] M. P. De Jong, L. J. Van Ijzendoorn, M. J. A. De Voigt, *Appl. Phys. Lett.* **2000**, *77*, 2255.
- [19] S. R. Dupont, M. Oliver, F. C. Krebs, R. H. Dauskardt, *Sol. Energy Mater. Sol. Cells* **2012**, *97*, 171.
- [20] T. Ye, W. Chen, S. Jin, S. Hao, X. Zhang, H. Liu, D. He, *ACS Appl. Mater. Interfaces* **2019**, *11*, 14004.
- [21] A. L. Shu, A. Dai, H. Wang, Y. L. Loo, A. Kahn, *Org. Electron.* **2013**, *14*, 149.
- [22] A. Dai, Y. Zhou, A. L. Shu, S. K. Mohapatra, H. Wang, C. Fuentes-Hernandez, Y. Zhang, S. Barlow, Y. L. Loo, S. R. Marder, B. Kippelen, A. Kahn, *Adv. Funct. Mater.* **2014**, *24*, 2197.
- [23] F. Guillain, J. Endres, L. Bourgeois, A. Kahn, L. Vignau, G. Wantz, *ACS Appl. Mater. Interfaces* **2016**, *8*, 9262.
- [24] V. A. Kolesov, C. Fuentes-Hernandez, W. F. Chou, N. Aizawa, F. A. Larrain, M. Wang, A. Perrotta, S. Choi, S. Graham, G. C. Bazan, T. Q. Nguyen, S. R. Marder, B. Kippelen, *Nat. Mater.* **2017**, *16*, 474.
- [25] Y. Lin, B. Adilbekova, Y. Firdaus, E. Yengel, H. Faber, M. Sajjad, X. Zheng, E. Yarali, A. Seitkhan, O. M. Bakr, A. El-Labban, U. Schwingenschlögl, V. Tung, I. McCulloch, F. Laquai, T. D. Anthopoulos, *Adv. Mater.* **2019**, *31*, DOI 10.1002/adma.201902965.
- [26] J. Hu, W. Fu, X. Yang, H. Chen, *J. Polym. Sci.* **2022**, *32*, 1.
- [27] H. Xu, H. Zou, D. Zhou, L. Zhang, X. Liao, L. Chen, Y. Chen, *ACS Appl. Mater. Interfaces* **2021**, *13*, 39844.
- [28] C. Sun, F. Pan, H. Bin, J. Zhang, L. Xue, B. Qiu, Z. Wei, Z. G. Zhang, Y. Li, *Nat. Commun.* **2018**, *9*,

1.

- [29] W. Gao, A. Kahn, *J. Appl. Phys.* **2003**, *94*, 359.
- [30] A. I. Hofmann, R. Kroon, S. Zokaei, E. Järsvall, C. Malacrida, S. Ludwigs, T. Biskup, C. Müller, *Adv. Electron. Mater.* **2020**, *6*, 1.
- [31] W. Zhao, S. Li, H. Yao, S. Zhang, Y. Zhang, B. Yang, J. Hou, *J. Am. Chem. Soc.* **2017**, *139*, 7148.
- [32] Q. Fan, W. Su, Y. Wang, B. Guo, Y. Jiang, X. Guo, F. Liu, T. P. Russell, M. Zhang, Y. Li, *Sci. China Chem.* **2018**, *61*, 531.
- [33] X. Li, J. Yao, I. Angunawela, C. Sun, L. Xue, A. Liebman-Pelaez, C. Zhu, C. Yang, Z. G. Zhang, H. Ade, Y. Li, *Adv. Energy Mater.* **2018**, *8*, 1.
- [34] T. Nicolini, A. V. Marquez, B. Goudeau, A. Kuhn, G. Salinas, *J. Phys. Chem. Lett.* **2021**, *12*, 10422.
- [35] M. M. Beerbom, B. Lägél, A. J. Cascio, B. V. Doran, R. Schlaf, *J. Electron Spectros. Relat. Phenomena* **2006**, *152*, 12.
- [36] Y. Zhang, B. De Boer, P. W. M. Blom, *Adv. Funct. Mater.* **2009**, *19*, 1901.
- [37] J. Euvrard, A. Revaux, P. A. Bayle, M. Bardet, D. Vuillaume, A. Kahn, *Org. Electron.* **2018**, *53*, 135.
- [38] M. Urien, G. Wantz, E. Cloutet, L. Hirsch, P. Tardy, L. Vignau, H. Cramail, J. P. Parneix, *Org. Electron.* **2007**, *8*, 727.
- [39] I. E. Jacobs, E. W. Aasen, J. L. Oliveira, T. N. Fonseca, J. D. Roehling, J. Li, G. Zhang, M. P. Augustine, M. Mascal, A. J. Moulé, *J. Mater. Chem. C* **2016**, *4*, 3454.
- [40] Q. Fu, Y. Li, X. Wang, Q. Li, F. Wang, R. Yang, *J. Mater. Chem. C* **2020**, *8*, 17185.
- [41] T. Mori, X. Ma, H. Furuhashi, T. Nishikawa, *J. Photopolym. Sci. Technol.* **2013**, *26*, 377.
- [42] W. Liu, L. Müller, S. Ma, S. Barlow, S. R. Marder, W. Kowalsky, A. Köhn, R. Lovrincic, *J. Phys. Chem. C* **2018**, *122*, 27983.
- [43] S. Zokaei, D. Kim, E. Järsvall, A. M. Fenton, A. R. Weisen, S. Hultmark, P. H. Nguyen, A. M. Matheson, A. Lund, R. Kroon, M. L. Chabinyk, E. D. Gomez, I. Zozoulenko, C. Müller, *Mater. Horizons* **2022**, *9*, 433.
- [44] A. Dai, A. Wan, C. Magee, Y. Zhang, S. Barlow, S. R. Marder, A. Kahn, *Org. Electron.* **2015**, *23*, 151.